BEHAVIOUR OF POLYMERIC MULTISCALE FOAM UNDER DYNAMIC LOADING -STUDY OF THE INFLUENCE OF THE DENSITY AND THE WALLS OF BEADS

P. Viot[1,2,*], L. Mah´eo[1] & A. Mercier[2]

[1]Arts et Metiers ParisTech, I2M-DuMAS UMR 5295 CNRS, Esplanade des arts et metiers, 33405 Talence cedex, France
[2]Institut Superieur Industriel de Bruxelles, LMA, H.E. P.-H. Spaak, Brussels, Belgium
***E-mail:** philippe.viot@ensam.eu, ***Tel.:** +33 5 56 84 53 62, ***Fax:** +33 5 56 84 53 66.

ABSTRACT

Polymeric foams constituted of large beads and microscopic cells are used in a number of applications of passive safety. Previous experimental studies had shown that the heterogeneity of the bead density and the network constituted of bead walls have an influence on the foam behaviour. A numerical approach has been developed to model the local behaviour of multiscale structure of a polymeric foam. The objective of this study is to estimate the influence of the cell microstructure and the bead wall structure on the macroscopic response of the foam and moreover to explain the phenomena of bead wall buckling and strain localisation bands observed experimentally. Numerical simulations (in LS-Dyna) have been carried out in order to implement the two sizes of the foam morphology, the mesoscopic scale of beads were represented by a dense wall structure (the thickness of the walls is one of the parameter of the modelling) and the behaviour of microscopic cells was represented by a classical model of cellular material (implemented in FE code and experimentally identified). A design of experiment was established to better identify the influence of each parameter -thickness of the wall, bead density and mean strain- on the local and global response of the multiscale structure.

Keywords: *Foams, Impact behaviour, Computational modelling, Microstructures.*

1. INTRODUCTION

Polymer foams are used in a number of applications of passive safety for consumer goods (packaging for electronic equipment...) or for consumers themselves (helmets, knee pads...) because of their good energy absorbing capability during a shock. Classically, the behaviour of these foams under compression presents three regimes [1,2]: an elastic behaviour followed by a stress plateau (where the stress is nearly constant for a large range of strain) and finally a densification step. The two first stages have to be particularly well identified to improve the design of the parts made in foam. For instance, the cellular materials used in packaging must resist to the weight of the transported equipment (the elastic rigidity of the foam must be quantified) and they have also to dissipate energy to protect the equipment from shock as well as possible (the stress plateau must be identified).

A numerical modelling approach can be considered to improve the performance of these structures. Constitutive models have already been investigated for cellular materials: their behaviour is usually characterized as functions of foam density, strain rates, temperature, etc... in applying rheological tests such as dynamic uni axial compression, hydrostatic compression [3,4,5] or more complex loadings [6]. Some of these behaviour models have already been implemented in Finite Element software codes such as Abaqus [7] and LS-Dyna [8] and are already used by research department to numerically estimate the foam structure response under static and dynamic loadings.

However, these macroscopic models do not take into account the real morphology of the foam structure and they can not represent the localisation of the deformation observed experimentally [9] (see figures 1 and 2). A first strategy to model the strain heterogeneity of cellular material is to represent the microstructure by regular uniform cells or beads. Gibson and Ashby [1] established constitutive equations based on the analysis of the mechanical response of a foam ideal structure constructed from cubic cells. Kraynik and Warren [10] purposed a phenomenological model in describing the deformation of the arrangement of tetrakaidecahedral cells representing more precisely the shape of closed cells. Mills and Gilchrist [11] purposed numerical modelling of regular packing of uniform-sized beads by taking into account the gas flow in the foam structure. However, from these approaches, the influence of the variability of shape and size of the cells on the macroscopic behaviour can not be estimated. Another strategy is to generate random structures of cells from Voronoi tessellation. Roberts and Garboczi [12] created three-dimensional Voronoi models of open-cell foams. The foams of this study are issued from an industrial process; bead geometry is complex and some defaults in the cell structure such as large air bubbles included in the porous material can be observed. It is then more difficult to generate this kind of structure with Voronoi model.

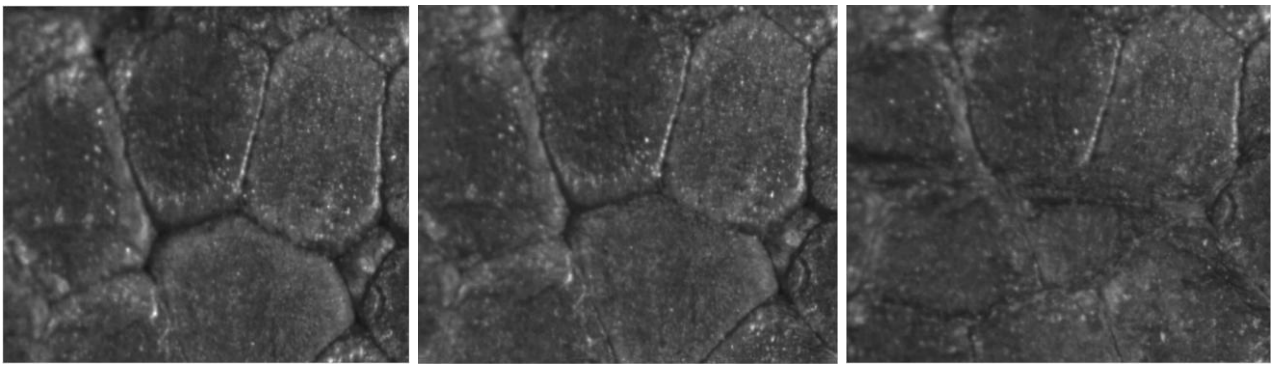

[t = 0 ms.] [t = 2.5 ms.] [t = 5 ms.]

Figure1: Three pictures extracted of a dynamic compression test of a polypropylene (PP) foam with a punch velocity of 2 $m.s^{-1}$.

Finally, manufacturing processes can generate a more complex microstructure [2] (see figure 1a); expanded plastic foam beads are injected in a mold where the individual beads are expanded and fused together under steam heat and pressure [13]. In consequence the structure of these foams (classically used in structural parts) is multiscale; the beads are millimetric (about 2 to 5 mm for polypropylene or polystyrene foams) and they are made of microscopic closed cells (figure 2a). The cell walls are no more than a micron thick whereas the walls of the beads are thicker (about a tenth of a millimetre). The effect of the walls of the beads on the cellular material behaviour has to be considered. It seems evident that these thicker walls constitute a more rigid secondary network which have an influence on the local deformation of the microstructure (at the cell scale) and its macroscopic response. Moreover, a previous experimental study has shown that the heterogeneity of bead density in this industrial polypropylene foam induces a difference of rigidity between beads and consequently a non-homogeneous deformation of the structure [14].

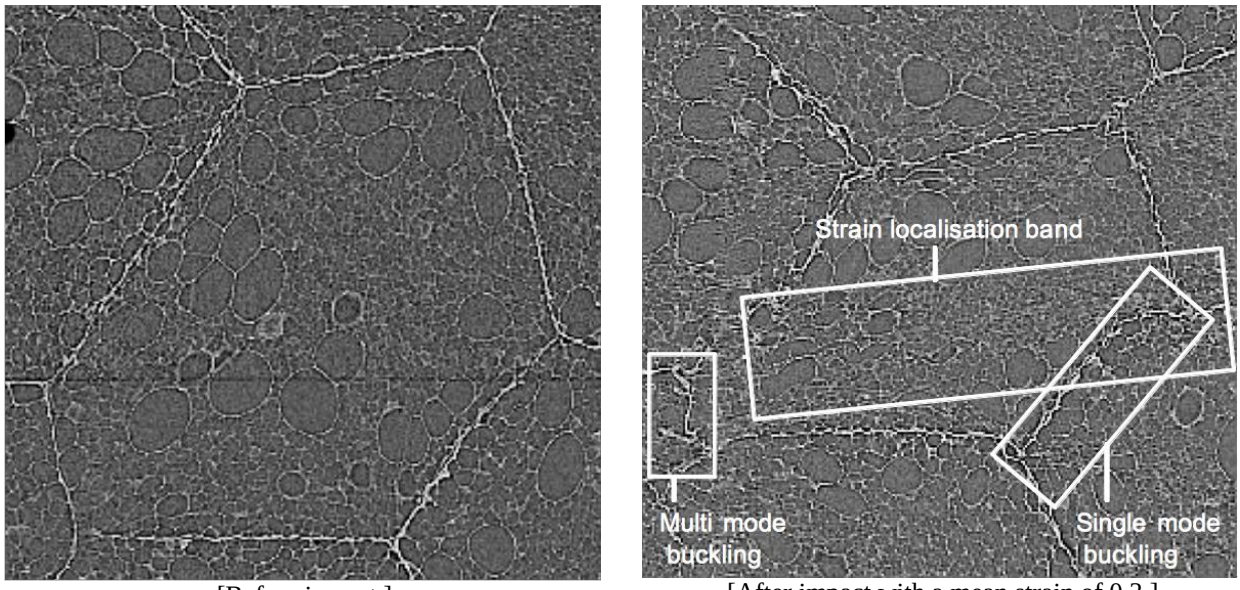

[Before impact.] [After impact with a mean strain of 0.3.]

Figure2: Local microstructure of a PP foam (obtained using microtomography) before and after a dynamic compression test.

For multiscale foams, a multiscale approach must be investigated in order to model the two sizes of the foam morphology, the mesoscopic scale of beads and the microscopic one of cells. A complete modelling approach of this study would therefore consist in combining a Finite Element Model to represent the network of the bead wall and a modified Discrete Element Model to introduce the variability of the microscopic cell structure.

The first step of this research work which is presented in this paper is the modelling of the mesoscopic scale of the foam under dynamic loading in using FE technique. The walls of the beads are meshed as dense walls and their interior (constituted of cells) is a homogenised porous material. The objective of this step is to highlight the effect of the bead density and the wall thickness of the beads on the foam behaviour during a dynamic compression test. From simple numerical modelling, we want to reproduce and explain the complex physical phenomena which can appear during dynamic compression test such as strain localisation band in the interior of the bead (microscopic scale) and single or multi mode buckling (mesoscopic scale) of the walls of the beads (see figures 1 and 2).
A study of the influence of some parameters on the macroscopic and mesoscopic response of the foam have to be carry out before beginning the complex modelling of a 3-D structure; two parameters seem preponderant in the deformation of a polymeric foam sample under dynamic loading: heterogeneous field of density and the thicker walls of beads may have a significant effect on the strain field.
The objective of this article is to show the effect of the two parameters density and the walls of the beads on the strain localisation with a simplified 2-D structure to understand mechanichal phenomena of foams. This paper is written in four sections. In section 2 `Model and design of experiments', the foam behaviour model is presented using the works of Gibson and Ashby [1]. The volume including several beads is then defined in a FEM context. A design of experiment (DOE) is established to reveal the influence of these two parameters on macroscopic and mesoscopic behaviours. The results of these modelling are analysed and presented in section 3 `Results'. In section 4 `Conclusion', the results are summarized and future investigations are briefly presented.

2. MODEL AND DESIGN OF EXPERIMENTS

2.1 Model

The modelling of this structure in the FE software LS-Dyna requires the implementation of the behaviour of porous and bulk polymeric material. The objective of this study is to highlight physical phenomena which can appear in multiscale polymeric foam and not necessary to determine with accuracy the macroscopic behaviour of a specific cellular material. The characteristics of the elastic plastic model used to represent the bulk polypropylene behaviour of the bead wall are issued from the literature [1] and are resumed in table 1.

Characteristics	Values
Density ρ_{pp}	910 kg.m^{-3}
Young's modulus E_{pp}	1000 MPa
Poisson's ratio	0.22
Yield stress σ_{pp}	40 MPa
Plastic modulus	100 MPa

Table 1: Characteristics of the bulk polypropylene

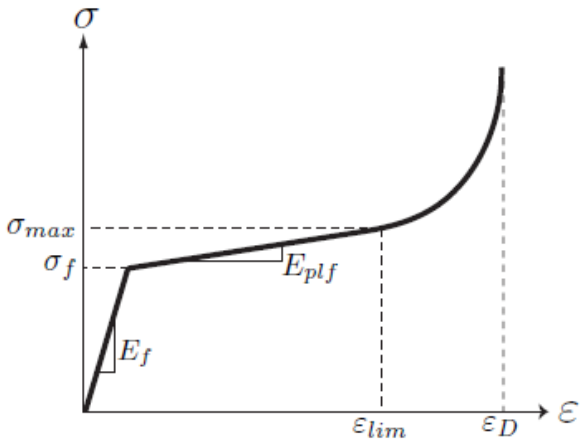

Figure 3: Scheme of cellular material behaviour (based on Gibson's model [1]).

Secondly, a classical model developed by Gibson and Ashby [1] was used to represent the behaviour (elastic - plateau plastic - densification) of the porous polypropylene subjected to compressional loads (see figure 3). The elastic behaviour is characterised by the Young's modulus E_f of the foam. For these first modelling, this parameter depends on the density ρ_f and can be obtained by:

$$\frac{E_f}{E_{pp}} = \phi^2\left(\frac{\rho_f}{\rho_{pp}}\right)^2 + (1-\phi)\left(\frac{\rho_f}{\rho_{pp}}\right) \quad (1)$$

where E_{pp} and ρ_{pp} are respectively the Young's modulus and the density of the polypropylene (see table 1) and ϕ is a coefficient depending on the geometry of the cells [1]. For the polypropylene foam of this study, this coefficient was evaluated to $\phi = 0.1$ by Viot et al.[15].

The limit of the elastic behaviour is characterised by the yield stress of the foam σ_f empirically established from the relation:

$$\frac{\sigma_f}{\sigma_{pp}} = \frac{1}{2}\phi^{\frac{3}{2}}\left(\frac{\rho_f}{\rho_{pp}}\right)^{\frac{3}{2}} + \frac{2}{5}(1-\phi)\left(\frac{\rho_f}{\rho_{pp}}\right) \quad (2)$$

where σ_{pp} is the yield stress of the polypropylene (see table 1). The plastic behaviour of the cellular material can be characterized by the slope of the plateau in the diagram stress vs. strain. This increase in the stress is due to the rigidity of the structure of the foam (in the plastic phase). Gibson and Ashby [1] consider that the stress (due to the buckling of the cell walls) is constant during the plastic plateau. However, static and dynamic compressions on polypropylene foams of several densities (25, 70, 80, 90 and 180 kg.m^{-3}) have shown that the stress increases significantly in function of the irreversible strain and the slope of the plastic plateau can be estimated from the plastic modulus E_{plf}. From these experimental results, we considered that this parameter can be correlated to the Young's modulus E_f of the foam:

$$E_{plf} = \frac{E_f}{K_E} \quad with \quad K_E = 50 \quad \text{experimentally identified by [5]} \quad (3)$$

It has been shown that the plastic modulus E_{plf} depends on the density [5]. The stiffness of the cellular material is higher because either the cell number is more significant or the cell walls are thicker. In equation 3, the plastic modulus E_{plf} depends on the density because the Young's modulus E_f is a function of this parameter (equation 1). The coefficient K_E is established to take into account the loss of stiffness between the elastic and plastic behaviours. During plastic plateau, the damage phenomena observed on this polypropylene foam is the buckling of cell wall. The rigidity of the cell walls in buckling is significantly lower than their rigidity in compression.

For the final phase of densification, the stress increases exponentially from a value of irreversible strain ε_{lim}. Gibson [1] defined a relation to establish this strain value from which the densification begins:

$$\varepsilon_{lim} = \varepsilon_D\left(1 - D^{-\frac{1}{m}}\right) \quad with \quad \varepsilon_D = 1 - 1.4\left(\frac{\rho_f}{\rho_{pp}}\right) \quad (4)$$

where ε_D is the full densifications strain. The coefficients D = 2.3 and m = 0.8 are empirical parameters and were experimentally determined by Bouix et al.[5].

Finally, the stress variation is established by Gibson [1] as a function of the strain during the densification:

$$\sigma = \frac{\sigma_{max}}{D}\left(\frac{\varepsilon_D}{\varepsilon_D - \varepsilon}\right)^m \tag{5}$$

with ε_D determined in the equation 4 and σ_{max} corresponds to the stress at the beginning of the densification. It can be calculated from the yield stress σ_f and the slope of the plastic plateau determined from the equation 3.

$$\sigma_{max} = \sigma_f + \frac{E_f}{K_E}\varepsilon_{lim} \tag{6}$$

Experimental data obtained from compression tests on polypropylene foams of several densities (25, 70, 80, 90 and 180 kg.m^{-3}) allowed determining the characteristics of the foam model (used in LS Dyna) as a function of density (figure 4).

Although previous studies [9] have shown the sensitivity of the foam behaviour to the strain rate and the localisation of the strain induces necessarily a local variation of the strain rate, the effect of the strain rate is not taken into account for this first modelling. A future work will deal with this effect.

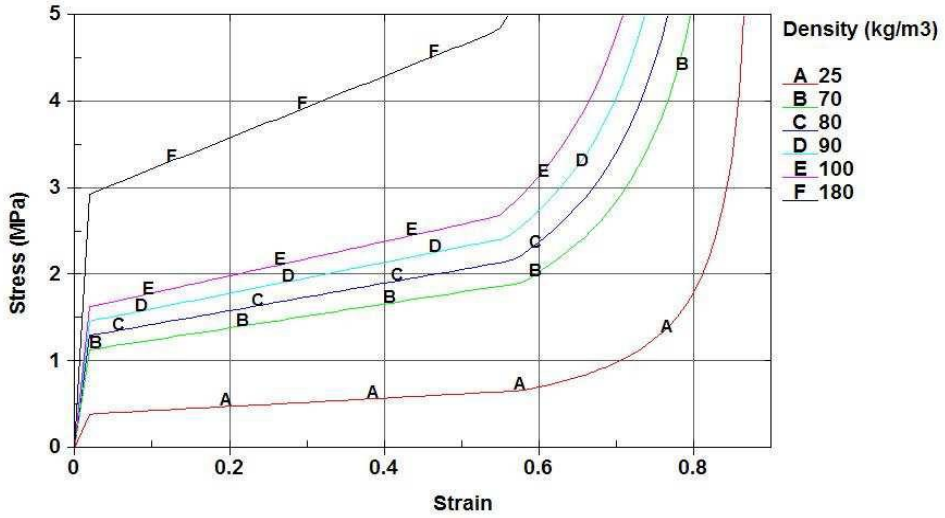

Figure 4: Compressive behaviour of PPE foam depending on foam density.

2.2 Numerical modelling

The finite element model has been developed to be suitable for analysis with LS-Dyna. The influence of the two parameters bead density and walls of the beads on the strain localisation is studied using a simplified 2-D structure composed of seven beads to understand mecanichal phenomena of foams.

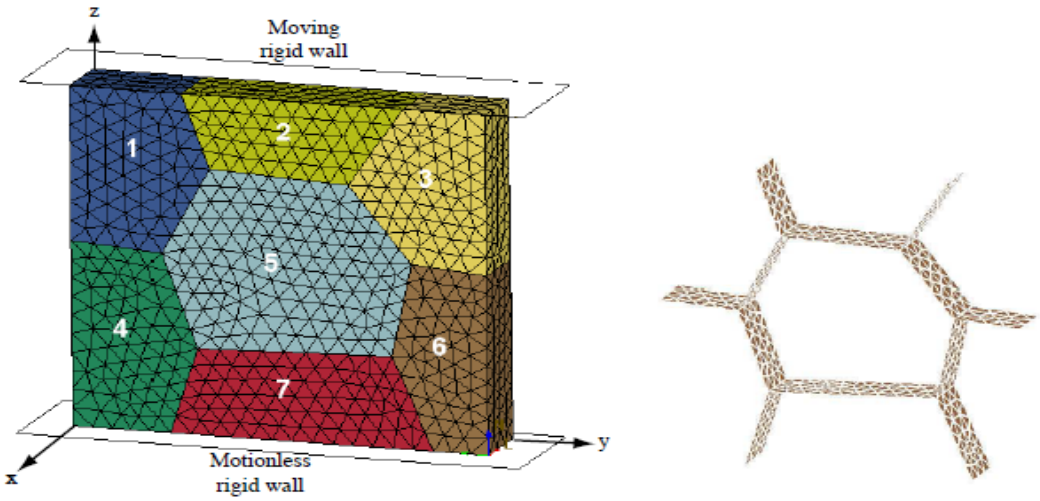

[The beads are discretised into solid elements.] [The wall network of the beads is discretised into shell elements.]

Figure 5: Finite Element model of the beads structure.

2.2.1 Spatial and time discretisations

Seven beads are discretized into 3-D constant stress solid elements and the wall network between the beads is modeled by 2-D Belytschko-Tsay shell elements (see. figures 5). The average edge size of those seven beads is 0.3 mm. This set of 7 beads constitutes a parallelepipedic volume of dimensions $1.0 \times 6.0 \times 5.5\ \text{mm}^3$.
The integration scheme used in LS-Dyna software is the explicit Central Finite Difference. The time step duration fluctuates between $4.5 \cdot 10^{-9}$ and $1.4 \cdot 10^{-8}$ s for all the calculations.

2.2.2 Loading and boundary conditions

Two rigid walls allow us to represent the compression punches. Only the upper one is moving, with an initial velocity of $2\ \text{m.s}^{-1}$ in the negative vertical $\vec{z}$ direction (see. figure 4). Regarding the boundary conditions for this FE model, a friction coefficient of 1 has been set between the rigid walls and the beads. Furthermore, the translational displacement of the front face nodes and the back face nodes has been restrained in the $\vec{x}$ direction. The right and left face nodes are likewise restrained in the $\vec{y}$ direction.

2.2.3 Numerical material behaviour

The material model *MAT_LOW_DENSITY_FOAM (*MAT_057) which is the same one as in Croop and Lobo [16] is chosen to model the behavior of the seven beads. The numerical inputs of this model are the density of the foam ρ_f, the Young modulus of the foam E_f and the stress-strain curve which defined the compressive behavior of the foam (see figure 3). One of the main advantage using this model is therefore to directly import stress-strain curves from experimental data. The selected curves used are presented figure 4. The density of the beads located around the bead number 5 is fixed to $70\ \text{kg.m}^{-3}$ throughout the study whereas the density of the bead number 5 can be singly adjusted to study its effects on the strain localisation.
The wall network between the beads is modeled with the elasto-plastic material model *MAT_PIECEWISE_LINEAR_PLASTICITY (*MAT_24). As mentioned before, the material parameters for those bead walls are issued from the literature [1] and are resumed in the table 1. In order to avoid the contact algorithms definition and computation, and to better-represent the real interface between the beads, we have decided to merge the nodes of the bead walls with the related beads ones. The thickness of the wall network can be easily adjusted to show its influence on the strain localisation.

2.3 Design of experiments

The objective of this part of the study is to highlight the influence of some parameters such as the density of beads in the foam, the thickness of the walls of the beads as a function of the mean strain imposed during the dynamic loading. Due to the fact that there are several factors which may influence the response of a foam sample, a large number of tests needs to be conducted before any trends relating the response to each influencing parameter may be extracted. Therefore, it seems difficult to establish mechanical relations associating, for instance, the heterogeneity of the strain field for a mean strain imposed and for different values of bead wall thickness and bead density. The use of design of experiments (DOE) methods is an alternative to provide an empirical response surface between the consequence (heterogeneity of the strain field and creep) and the causes (variability in the density, thickness of bead wall, mean strain). This method allows the simultaneous investigation of the influence of several variables -and their interactions- on the response; it limits the number of tests and provides results with a good accuracy [17,18].
In consequence, a design of experiments had been used to establish an empirical response surface showing the heterogeneity of the strain field in the specimen as a function of three factors, the density ρ of the bead in the centre of the specimen, the thickness e of the mesoscopic and the mean strain ε_z imposed during the dynamic loading. Two factors were proposed to indicate the heterogeneity of the strain field ε_z during an uni-axial compression. The first one Y_1 is a coefficient of axial strain variation divided by the mean of axial strain:

$$Y_1 = \frac{\varepsilon_{z.max} - \varepsilon_{z.min}}{\varepsilon_{z.mean}} \tag{7}$$

Y_1 is weak if the difference between maximal and minimal strain measured in the sample is negligible compared to the mean strain imposed. A second factor Y_2 which can indicate the heterogeneity of the axial strain field ε_z is the creep ε_{yz} in the plane yz. It has been shown that creep can locally appear in the structure as the axial strain becomes heterogeneous. For a structure under an uni-axial compression test, the local value of the strain ε_{yz} in a point M of the structure is then a good indicator of the localisation of the strain in this point. The second factor Y_2 chosen to indicate the heterogeneity of the axial strain field is the maximal value of the strain ε_{yz}. These two factors indicate a global heterogeneity of the axial strain field, and they do not allow estimating the local gradient of deformation; it is then necessary to complete this study in analysing directly the strain fields when the two factors Y_i reveal the presence of any heterogeneity.

The design of experiment has to establish two response surfaces Y_1 and Y_2 as functions of the three factors, the density ρ, the wall thickness e and the mean strain ε_z.

Many different models can be established to represent the factor response ($Y_{i=1or2}$) as a function of the three parameters (ρ, e and ε_z). A quadratic model is classically used in this kind of method [18] and its identification can be obtained using a 3 factors Box-Benkhen Design. The polynomial function is not directly estimated from the physical parameters but from non-dimensional variables. Each input parameter (ρ, e or ε_z) is expressed in terms of a centered and reduced non-dimensional variable X_j by the equation :

$$X_j = \frac{u_j - u_j^0}{\Delta u_j} \tag{8}$$

where u_j is the value of the corresponding physical parameter, u_j^0 the mean value of the physical parameter and Δu_j, the variation step, which is calculated from:

$$\Delta u_j = \frac{u_{j.max} - u_{j.min}}{2} \tag{9}$$

The maximal and minimal values of the physical parameters have been chosen to obtain non-dimensional centered variables X_j (table 2). However, the variable X_1 corresponding to the foam density is non centered (its range is [-0.72;1]); the macroscopic behaviour was established from Gibson model [1] and verified on polypropylene foam of several values of density 25, 70, 80, 90, 100 and 180 kg.m^{-3}, and these results are used to identify the model implemented in LS-Dyna. It is then necessary to choose 3 values of density from these 6 values to determine the domain in density of the DOE. The Box-Benkhen Design matrix was modified to take into account this constraint. Once these variables have been established, it is postulated that the response surface ($Y_{i=1or2}$) is represented by a polynomial function:

$$Y_{i=1or2} = \sum_{i,j=1}^{3} (b_0 + b_i X_i + b_{ij} X_i X_j) \tag{10}$$

X_j	j	u_j	$u_{j.min}$	u_j^0	$u_{j.max}$	Δu_j	Range of u_i	Range of X_i
X_1	1: density (kg.m^{-3})	u_1	0	90	180	90	[25;180]	[-0.72;1]
X_2	2: thickness (mm)	u_2	0.0	0.1	0.2	0.1	[0.0;0.2]	[-1;1]
X_3	3: mean strain	u_3	0.1	0.3	0.5	0.3	[0.1;0.5]	[-1;1]

Table 2: Range of the three input parameters

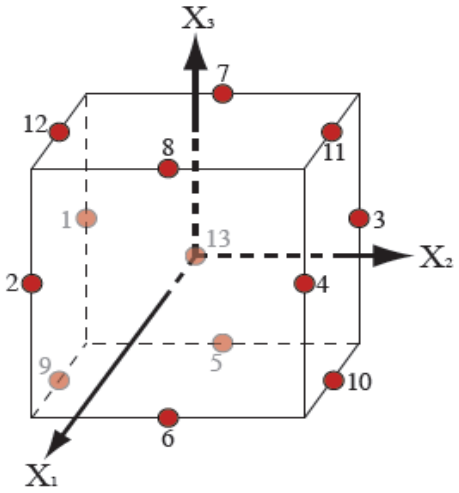

Figure 6: Location of the tests in the space (X_1, X_2, X_3)

The software NEMRODW (from LPRAI Laboratory, Marseille, France) was used to create the Box-Benkhen Design matrix and identify the quadratic model. The coefficients b_{ij} of the polynomial function were determined by carrying out the tests shown table 3 and figure 6. With this kind of experiment, only 13 numerical tests are indispensable to determine the coefficients b_{ij}. The first twelve experiments are on the surface of a sphere, at equal distance from the centre point (see experiments 13 and 14 in table 3 and figure 6). Complementary simulations were calculated in the corners of the domain (experiments 15 to 22) to improve the accuracy of the model (established from the variance). Hence, the experiments 23 to 26 are implemented to take into account the fact that for a homogeneous density on the volume (the bead 5 has the same density than the other ones) and the wall thickness e equal to zero, the strain field is necessarily homogeneous (Y_1 and ε_{yz} = 0). All these tests were characterized from the values of density ρ, wall thickness e and mean strain ε_z (X_1, X_2 and X_3, respectively). Hence, the two last columns of this table are the response factors Y_1 and Y_2 determined for each numerical simulation.

N Exp	Density (kg.m^{-3})	Thickness (mm)	Mean strain		
	u_1	u_2	u_3	Y_1	Y_2
1	25	0.0	0.3	1.50	0.12
2	180	0.0	0.3	1.50	0.13
3	25	0.2	0.3	2.37	0.49
4	180	0.2	0.3	2.62	0.40
5	25	0.1	0.1	5.07	0.33
6	180	0.1	0.1	5.49	0.23
7	25	0.1	0.5	1.50	0.44
8	180	0.1	0.5	1.52	0.47
9	90	0.0	0.1	1.68	0.04
10	90	0.2	0.1	7.88	0.37
11	90	0.0	0.5	0.10	0.02
12	90	0.2	0.5	1.83	0.46
13	90	0.1	0.3	2.57	0.35
14	90	0.1	0.3	2.57	0.35
15	180	0.0	0.1	2.40	0.08
16	180	0.0	0.5	0.49	0.07
17	180	0.2	0.1	7.27	0.32
18	180	0.2	0.5	1.80	0.32
19	25	0.0	0.1	2.92	0.43
20	25	0.0	0.5	0.27	0.06
21	25	0.2	0.1	7.98	0.38

22	25	0.2	0.5	1.84	0.48
23	70	0.0	0.1	0.00	0.00
24	70	0.0	0.3	0.00	0.00
25	70	0.0	0.5	0.00	0.00

Table 3: Box-Benkhen Design and results

3. RESULTS

The results of the numerical simulations allow identifying the polynomial functions corresponding to the Y_i response surfaces. These quadratic functions can be defined from Eq. 10 with the coefficients resumed table 4.

Coefficients	Value of Y_1	Value of Y_2
b_{00}	2.414	0.347
b_{01}	-0.063	-0.071
b_{02}	1.426	0.142
b_{03}	-1.969	0.005
b_{11}	0.133	0.069
b_{22}	-0.430	-0.103
b_{33}	0.967	-0.020
b_{12}	-0.054	-0.001
b_{13}	0.094	0.037
b_{23}	-0.960	0.049

Table 4: Coefficients values for the Y_i responses

The analysis of the b_{ij} values gives first informations on the effect of the three factors on the strain localisation: the relative influence of the parameter X_j can be estimated from the coefficients b_{0j} and b_{jj} and the coupling between two parameters X_i and X_j is evaluated from the value of the coefficient b_{ij}. If it is delicate to conclude from the coefficient b_{ij} of the Y_2 response, some first remarks can be done from the results obtained on the Y_1 response. The coefficients b_{02} and b_{22} are higher than respectively b_{01} and b_{11}, one shows that the thickness e of the bead wall has a more significant influence on the strain heterogeneity than the variability of the bead density. The effect of the strain imposed on the sample is also remarkable (b_{03} and b_{33} are the most high); it seems logical that the heterogeneity of the strain field is exacerbated for higher deformation. Therefore, the effect of the thickness of the bead wall and the strain imposed on the sample is coupling since the coefficient b_{23} is higher than the two other ones b_{13} and b_{12}. These results have to be confirmed in analysing the response surfaces Y_i and the strain field ε_z calculated in the plane yz. The following sections show the effect of the density, the influence of thickness e of the bead wall and the coupling between these two parameters.

3.1 Effect of the density

The effect of the density foam on the behaviour of cellular material have already been presented by many researchers at the bead scale [1,2,4,5]. The studies showing the bead density influence are more rare. This section presents the only density effect on the deformation of the foam volume without any coupling due to the parameter bead wall thickness in imposing $e = 0$.

The influence of the density on the meshed volume deformation is revealed on the response surface Y_1 and $Y_2 = \varepsilon_{yz}$ (figure 7). For the lower and higher density (ρ = 25 and 180 kg.m^{-3}) of the bead 5 (in the centre of the volume), the

coefficient Y_1 and the creep ε_{yz} are higher whereas their minimal value is reached for a density close to 70 kg.m^{-3}. The variation of Y_1 as a function of the bead density is relatively weak. On the contrary, the density influence of the creep ε_{yz} is particularly significant.

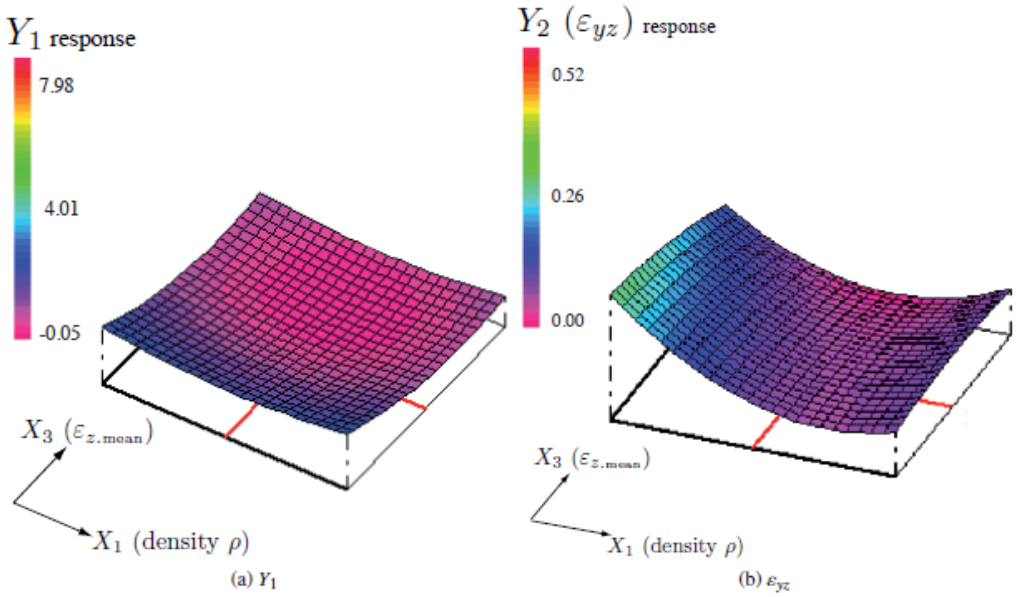

Figure 7: Dependency of the Y_1 and Y_2 parameters on density and mean strain

The minimum values for the responses Y_1 and Y_2 are obtained for a density close to 70 kg.m^{-3}. For this density equal to the density of the other beads, the strain field is homogeneous (the thickness of the bead wall is null and the density is constant on the complete volume) and consequently, the parameter Y_1 and the creep ε_{yz} are obviously equal to zero. The effect of the density heterogeneity on the strain field is presented figures 8 and 9 and corroborates the conclusions of the DOE results. These figures show the strain fields ε_z and ε_{yz} (respectively figures 8 and 9) for a mean strain = 10 % and for a central bead density of 25, 90, 180 (index a, b and c, respectively). For ρ = 25 kg.m^{-3}, the strain ε_z is obviously maximal in the bead 5 and is low in the upper and lower part of the meshed volume. In this case, the central bead is less rigid and resistant and it reaches firstly the state of plastic behaviour (the strain calculated in the centre of this bead is about -0.21, the twice of the mean strain imposed). Therefore, the compression stress is distributed to the neighbour beads (in the horizontal layer perpendicular to the compression axis) since the stress supported by the bead 5 is limited to the yield stress. This stress redistribution induces then a higher strain in the horizontal central layer including the less resistant bead. Equivalent comments can be done to explain the strain field (figure 7) calculated for a central bead density of 180 kg.m^{-3}. The bead 5 is more rigid and the upper and lower beads are then more deformed.

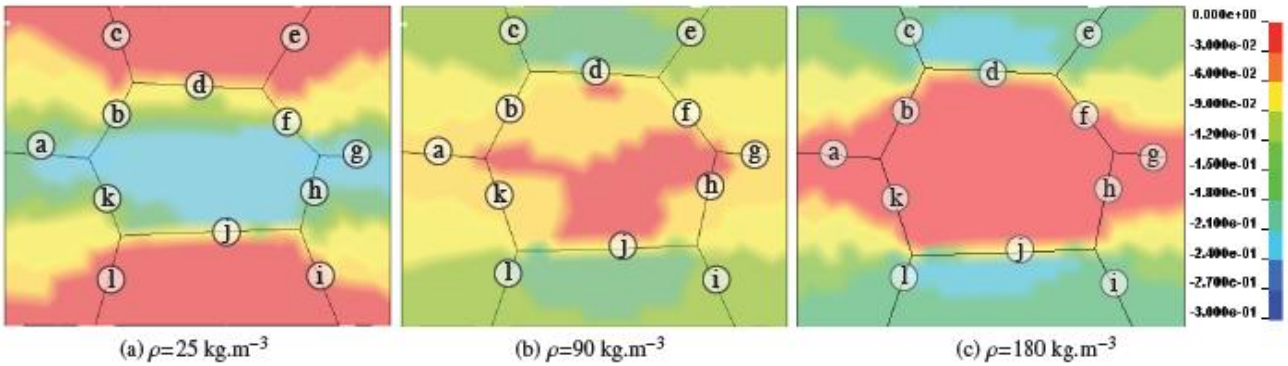

Figure 8: Strain field ε_z for three values of density of the central bead for an imposed strain of 0.1 ($t = 2.75 \cdot 10^{-4}$ s).

As regards the creep field ε_{yz}, the density heterogeneity induces a creep localization. The strain field depends on the density of the bead 5; the strain field obtained for a low density of the bead 5 (figure 8) is reversed from the one calculated for a density of 180 kg.m^{-3} (figure 8). However, the creep range is the same whatever the density of the central bead.

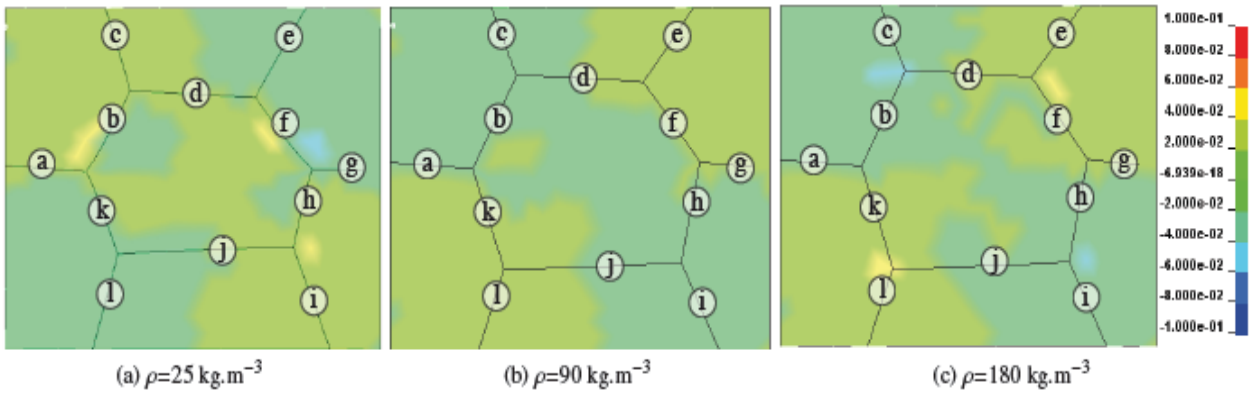

Figure 9: Creep ε_{yz} for three values of density of the central bead for an imposed strain of 0.1 ($t = 2.75 \cdot 10^{-4}$ s).

Moreover, the strain field is more heterogeneous at the beginning of the compression (for a mean strain ε_z of 0.1) and becomes low for significant mean strain ($\varepsilon_z > 0.5$). This result is confirmed in following the variation of Y_1 versus the mean strain ; it can be explained easily in taking for instance the case where the density of the bead 5 is 25 kg.m^{-3} (figures 10). At the beginning of the compression (figure 9), the difference of density between beads is highest and obviously its influence is significant. During the plastic plateau, the more deformed bead is the less dense (bead 5), the volume variation of this bead (of constant mass) induces an increase in both its density and its rigidity. For higher strain level (figure 9), the heterogeneity of density (and rigidity) is lower and the strain field is then more homogeneous.

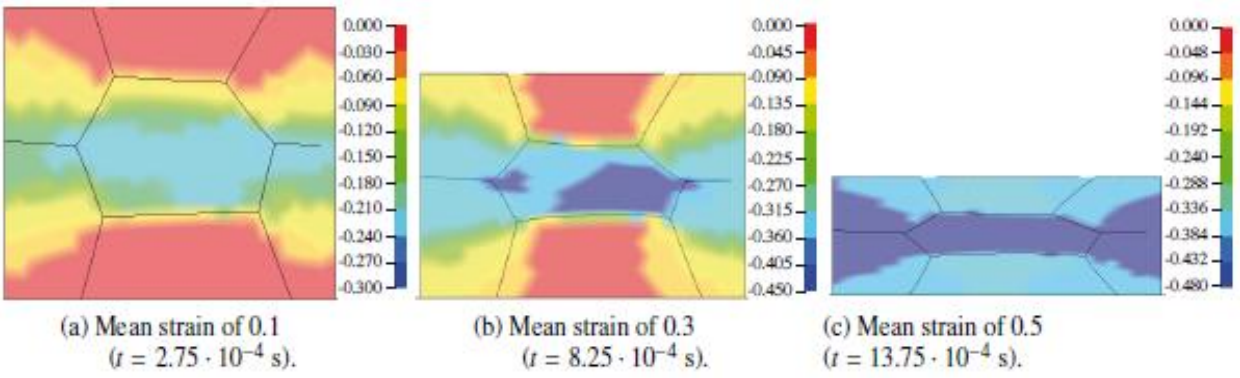

(a) Mean strain of 0.1 ($t = 2.75 \cdot 10^{-4}$ s). (b) Mean strain of 0.3 ($t = 8.25 \cdot 10^{-4}$ s). (c) Mean strain of 0.5 ($t = 13.75 \cdot 10^{-4}$ s).

Figure 10: Strain field ε_z for three values of mean strain

These first comments can be confirmed by analyzing the macroscopic response of this numerical cellular material (figure 11). The stress vs. strain curve obtained for a density of a 90kg.m $^{-3}$ (case 2) corresponds to a classical response of the cellular material. For a central bead density of 25 kg.m $^{-3}$ (case 1), the yield stress is normally lower than the one calculated for higher densities. However, for the density of 180 kg.m $^{-3}$ (case 3), the yield stress obtained is close to the one calculated for a density of 90 kg.m $^{-3}$. In these two cases (2 and 3), the yield stress of the complete cellular structure is limited by the yield stress of the less resistant beads (of density 70kg.m $^{-3}$). Consequently, the yield stress numerically obtained (about 1.2 MPa, figure 11) corresponds to the plastic stress value implemented in LS-Dyna for a density of 70 kg.m $^{-3}$. This explanation can not be done on the slope of the plastic plateau since the global plastic rigidity of the cellular structure is a combination of the assembled bead response. However, for a central bead density of 180 kg.m $^{-3}$, the plastic behaviour variation obtained for a strain close to 30 % can be explained easily by analyzing again the variation of the strain field during the compression. For a strain lower than this value, the macroscopic response of the cellular structure corresponds coarsely to the behaviour of the lowest density beads (beads 1, 2, 3, 4, 6 and 7) since they are the most deformed. From 30 % of strain, the increase in stress during the plastic plateau is due to the response of the central bead (of density 180 kg.m $^{-3}$) which becomes plastically deformed.

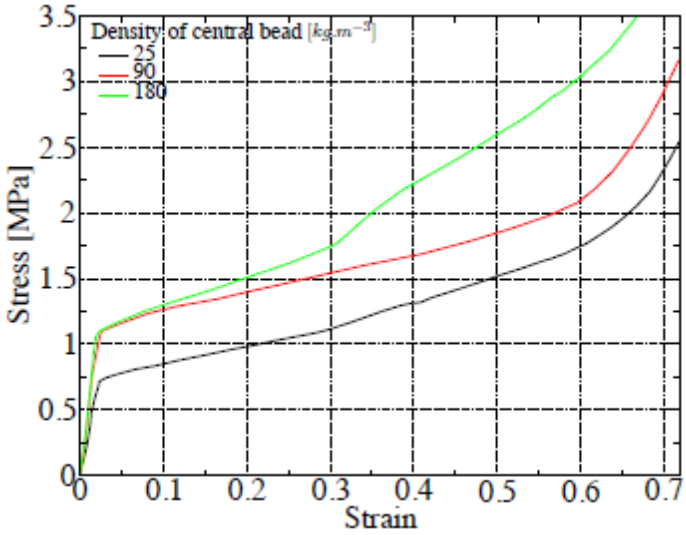

Figure 11: Stress vs. strain macroscopic response of the numerical sample for the three values of density of the bead 5

In first conclusion, the numerical simulations of the assembly of various density beads allow the explanation of the physical phenomena observed during experimental dynamic compression tests [5]. The heterogeneity of the strain field is directly due to the heterogeneity of the bead density (in the case where the bead wall thickness is null). The

modelling have also highlighted that this strain field heterogeneity decreases progressively during the compression to tend to zero for the densification phase. These results have been already experimentally identified on polypropylene foam under dynamic compression and now we show that the heterogeneous strain field can be due to the interaction between various density beads of the structure. The force field inside the microstructure is then more complex than the uni-axial compression numerically imposed. Moreover, all these results were confirmed by analyzing the macroscopic behaviour of the cellular structures. The stress-strain responses are due to a combination of the responses of various density beads. For lower mean strain, the less dense beads are more deformed and their responses affect directly the macroscopic behaviour. For higher strain, the behaviour of the cellular structure tends towards the response of the denser beads. From this numerical approach, we can reveal that the interaction between beads of different density generates high heterogeneous force field; the result can be observed locally on the strain field and more globally on the macroscopic response.

3.2 Effect of the wall thickness

The influence of the bead wall thickness was done in imposing a density of 90 kg.m $^{-3}$ for the central bead. The results of design of experiment reveal the evident effect of the thickness on the strain field heterogeneity (figures 12 and 13). The parameter Y_1 revealing the heterogeneity rate of the strain field is higher for the thicker bead wall. For lower mean strain $\varepsilon_{z.mean}$ (X_3 axis figure 12), the variation of the parameter Y_1 is significant; it is 7 times more significant for a wall thickness of 0.2 mm. Moreover this influence decreases as a function of the mean strain state of the material. Whatever the thickness, the heterogeneity appears higher for lower mean strain and reaches to the minimum values when the deformation state of the material tends to densification.

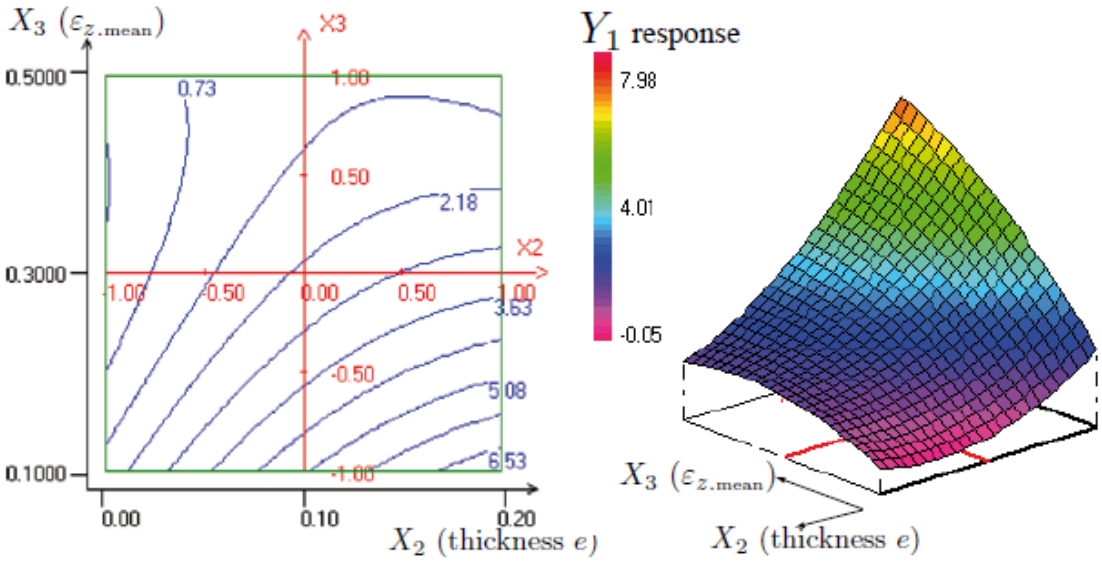

Figure 12: Dependency of the parameter Y_1 on thickness and mean strain

The effect on the creep ε_{yz} is also significant (figure 13). The maximum values are reached for higher thickness of bead wall. However, the ε_{yz} variation seems globally independent of the deformation state of the material / structure. One can consider that the creep field is initiated at the beginning of the compression (for lower value of deformation) and, this strain state being established, it is maintained until the densification.

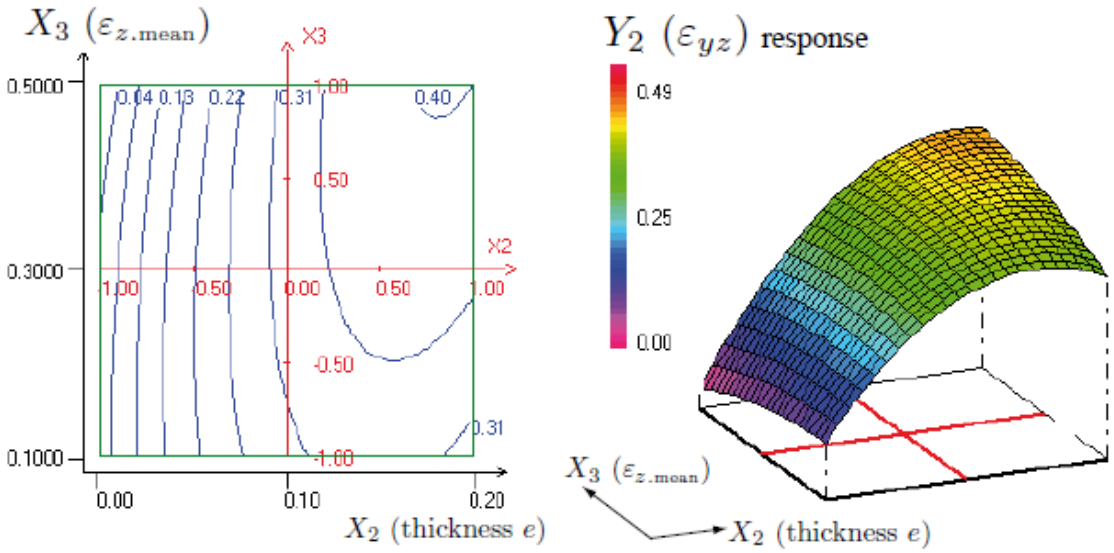

Figure 13: Dependency of ε_{yz} on thickness and mean strain

The analysis of the strain field allows the verification of these first conclusions on the influence of the walls of the beads. The strain field ε_z and the creep field ε_{yz} are presented respectively in figures 14 and 15 for three values of the wall thicknesses e 0.02, 0.1 and 0.2 mm (index a, b and c, respectively). These results are plotted for a mean strain of 10 %. For a wall thickness of 0.02 mm, the strain fields ε_z and ε_{yz} are relatively homogeneous. The effect of the wall is not relevant and the phenomena of buckling can not be yet visualized for this state of mean strain. The strain fields are significantly heterogeneous for thicker walls. Moreover, the strain fields depend on the value of the wall thickness e. For intermediate value e = 0.1 mm, the maximum strain ε_z is localized in a horizontal layer whereas the zone of maximum strain is more disturbed for e = 0.2 mm (figure 13). For intermediate thickness (figure 13), the buckling appears on the walls b and f localized in the same horizontal layer whereas it is the walls l and f which are damaged in the figure 13. During the compression, the stress is supported by the dense walls and the porous interior of the beads agglomerated. When the buckling appears on one of the walls of the structure, the stress supported by this wall is limited to the buckling stress and there is necessary a local redistribution of the stress on the porous structure. In consequence, a local increase in the strain ε_z appears close to this wall and the maximum strain zone progresses between buckled walls of the structure. The same conclusions can be done on the creep field ε_{yz}; for thicker walls, the maximum creeps appear close to the buckled walls. It seems evident since the local rotation of wall section induces necessarily a local shear stress state and then a creep strain.

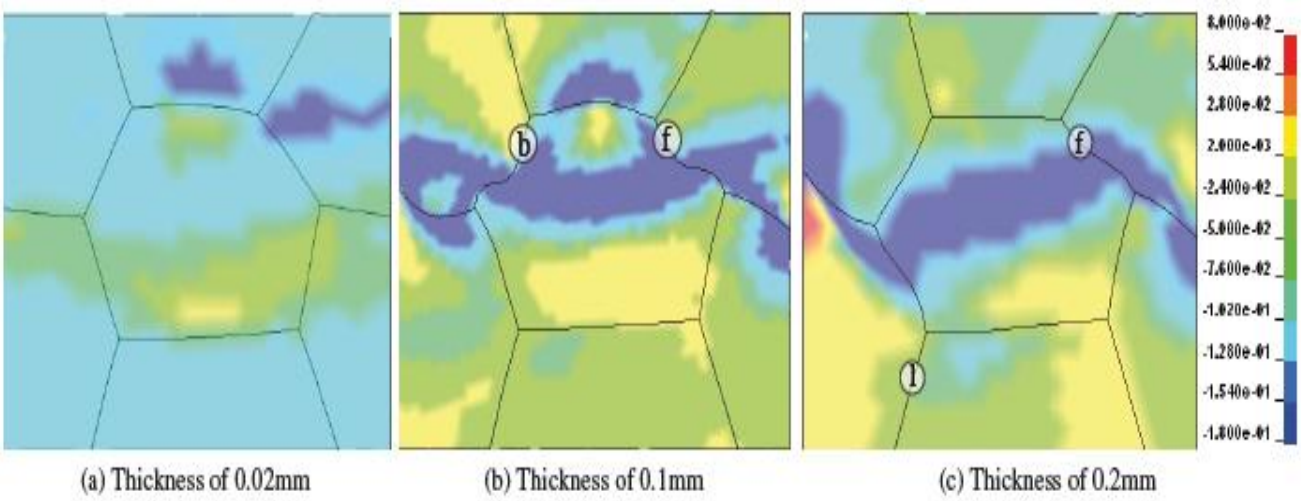

Figure 14: Strain field ε_z for three values of wall thicknesses for an imposed strain of 0.1 ($t = 2.75 \cdot 10^{-4}$ s).

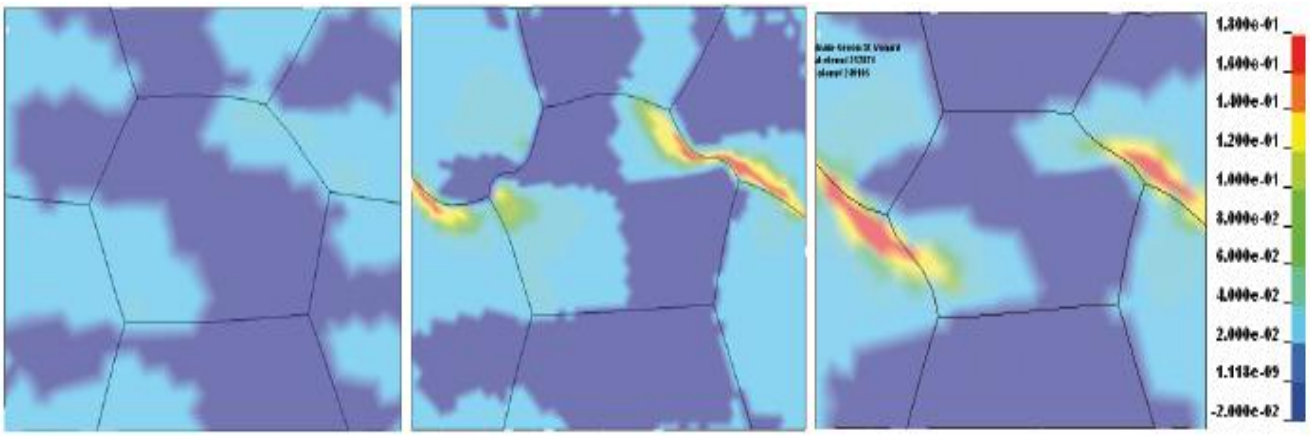

Figure 15: Creep ε_{yz} for three values of wall thicknesses for an imposed strain of 0.1 ($t = 2.75 \cdot 10^{-4}$ s).

To conclude on the analysis of the propagation of the damage in the structure, we can assume that the initiation of the buckling of few walls of the mesostructure induces local defaults of lower rigidity. This phenomenon generates a redistribution of the stress in the porous material and a localisation of the strain. Therefore, the strain localisation -and the damaged zone - can progress into the porous interior of beads and one can finally assist to a connexion of the different damaged zones which constitutes damaged layers observed on experimental video of dynamic compression.

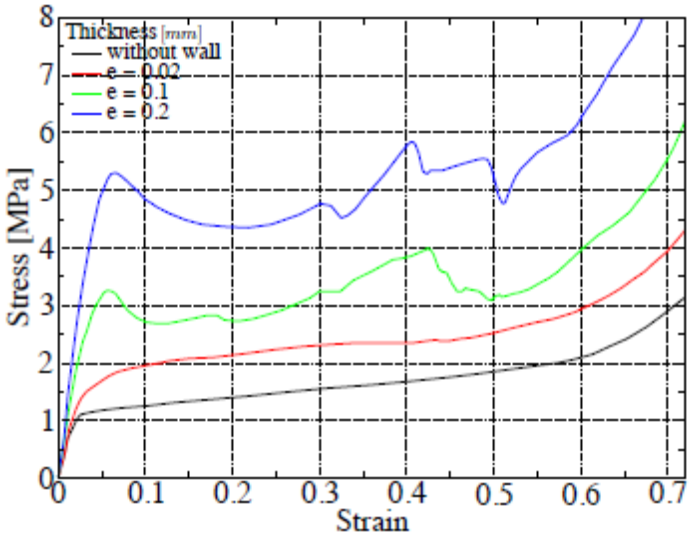

Figure 16: Stress vs. strain macroscopic response of the numerical for three values of wall thickness

Regarding the macroscopic response (figure 16), the thicker the walls of the beads, the higher the yield stress. The contribution of the bead walls to the rigidity and the resistance of the structure is significant. This comment seems evident since the mean density of the complete sample increases with the bead wall thickness. For thickness value lower than 0.1 mm, the transition between elastic and plastic response corresponds to the classical response of polymeric foam. Moreover, for higher thickness, the buckling phenomena can be detected by the peaks of the stress vs. strain curves. These curves are similar to the response observed in the case of metallic honeycomb or wood under uni axial compression (along the longitudinal axis of the material) where the buckling is the main phenomena of damage. The first peak shows that the bead wall structure more rigid allows the increase in the yield stress. The second peak corresponds to a buckling of another wall for higher mean strain. For a complete foam structure including hundreds of beads, peaks are multiple and appear stochastically; their cumulated effects lead to a classical foam response.

3.3 Coupling density/wall thickness

The last part of this study consists in analysing the coupling of the two parameters density and bead wall thickness on the mesoscopic behaviour. All the combinations can not be studied and it is the first advantage of design of experiment to obtain trends and conclusions on the cumulated effects of several parameters. The response Y_1 is calculated in the density - thickness plan ($X_1 - X_2$ plan) for three states of mean strain 0.1, 0.3 and 0.5 (respectively figures 16, 16 and 16).

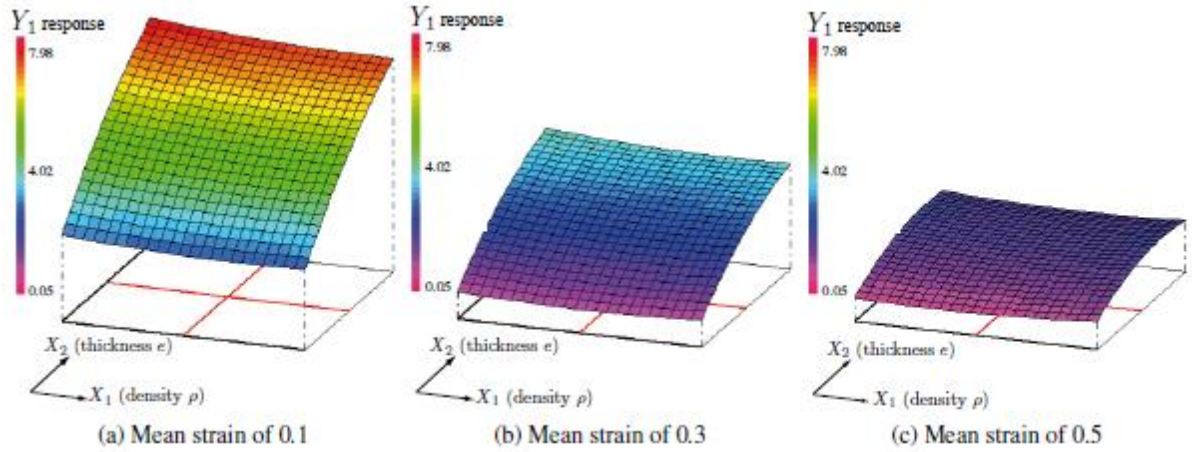

Figure 17: Dependency of the Y_1 parameter on thickness and density

First, the factor Y_1 (and then the heterogeneity in the strain field) decreases as a function of the mean strain. This result confirms the comments previously done. Second, it is obvious that the thickness has a more significant effect than the heterogeneity of the density (figure 16). The instability introduced by the buckling of the wall structure is the preponderant phenomena in the strain field heterogeneity.
In order to better estimate the influence of the coupling of the two parameters density and thickness on the strain field, the results obtained in the case of lower wall thickness are presented for two main reasons: firstly, this case is frequent in a lot of industrial foams and secondly if the thickness is higher, the effect of the variation of the density in the bead structure becomes negligible. The figures 18 and 19 reveal the strain field ε_z for a thickness of 0.02 mm and for a central bead density of 25, 90 and 180 kg.m^{-3} (respectively in the figures 17, 17 and 17). The results of strain field ε_{yz} were not presented since they give the same conclusions. These maps confirm the comments previously done on the strain heterogeneity: for a mean strain of 10 % (figure 17), it was confirmed that the strain field depends on the density of the central bead: the lower the density, the higher its strain state. Moreover, the buckling of the walls of the beads depends also on the density of the central bead. A significant density (higher than the density of the neighbouring beads) allows containing the wall buckling. On the contrary, for a density of 25 kg.m^{-3} (figure 17), the buckling of the wall **f** is initiated earlier and generates then a horizontal band of strain localisation which stretches in the lower bead density to the next bead wall (noted **b**). This wall **b** will be higher loaded and its buckling could be initiated (see figure 18).

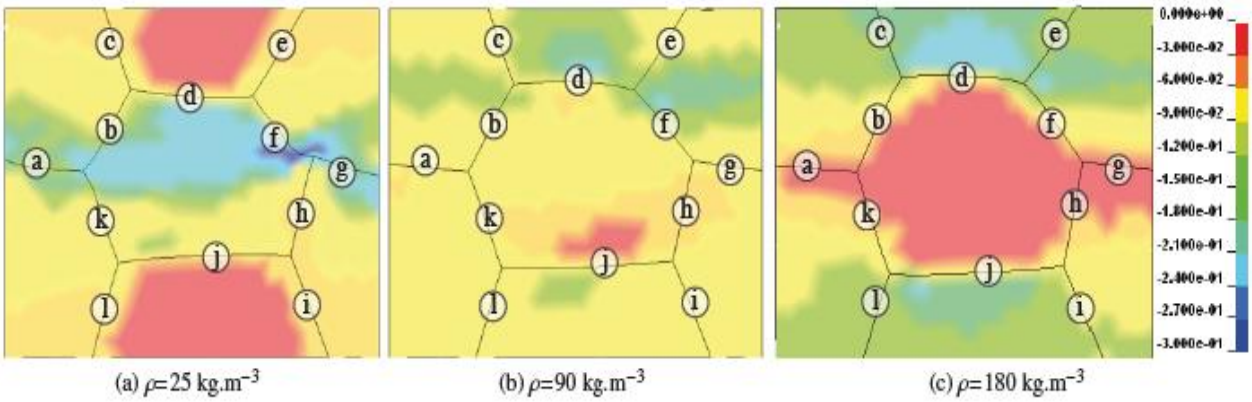

Figure 18: Strain field ε_z for three values of central bead density for an imposed strain of 0.1 ($t = 2.75 \cdot 10^{-4}$ s).

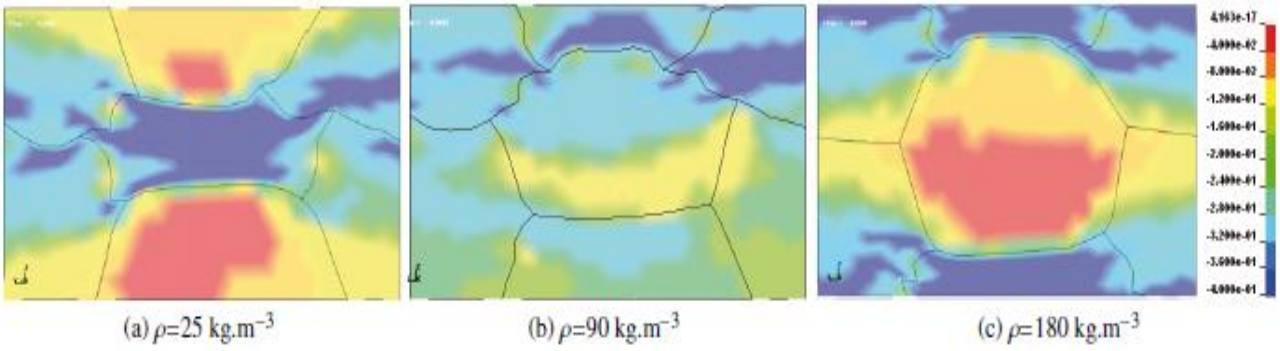

Figure 19: Creep ε_{yz} for three values of central bead density for an imposed strain of 0.3 ($t = 8.25 \cdot 10^{-4}$ s).

From this assumption, a process of damage propagation can be proposed. A lower bead density introduces a local weak behaviour which implies stress redistribution on the wall of this bead and then an instability on one of its wall. The wall buckling creates or amplifies a strain localisation which can spread in the lower density bead and generates the buckling of another wall. And so on. This damage kinetic can also be explained in term of stress. When the lower density bead behaviour becomes plastic, the stress applied on the bead is limited coarsely to the yield stress (in negligiting the plastic slope). Consequently, the stress in the bead neighbourhood and in the wall structure increases to

reach the buckling stress of one of the bead wall. The first buckling appears and implies a new stress redistribution. This damage propagation constituted of successive wall buckling and damage of the porous interior of beads can explain the deformation localisation in layers observed experimentally [9] during dynamic compression of multiscale polymeric foam.

This hypothesis can be easily verified in other configurations where the density of the central bead is higher than the other ones. The central bead, denser and then more resistant, can support higher stress. The upper and lower parts of the numerical sample are less rigid and the strain is the most significant in these zones (figures 17 and 17). The propagation of the damage is established in the same way and the heterogeneity of the strain field is particularly localised if the density difference between beads is high; the comparison between the strain field presented in the two figures 18 and 18 highlights clearly this phenomena whatever the state of mean strain. In last point, it is interesting to observe the occurrence of multi mode buckling in walls when the density difference is low between the two neighbouring beads. On the contrary, single mode buckling appears on walls between beads of high density variation. This phenomenon which can be easily explained by the theory of beam buckling had been already experimentally observed.

4. CONCLUSION

A numerical approach has been developed to model the local behaviour of multiscale polymeric foams constituted of large beads and microscopic cells. Many researchers have already analysed the influence of the cell microstructure on the macroscopic response of the foam but few studies were focussed on the cumulating effect of the two scales of foam structure constituted of microscopic cells localised in the bead interior and the bead wall network. The objective of this study is precisely to reveal this effect on the macroscopic response of the cellular material and furthermore to explain the phenomena of bead wall buckling and strain localisation bands observed experimentally.

For multi-scale foams, numerical simulations (in LS-Dyna) have been developed in order to implement the two sizes of the foam morphology, the mesoscopic scale of beads were represented by a dense wall structure (the thickness of the walls is one of the parameter of the modelling) and the behaviour of microscopic cells was represented by a classical model of cellular material (implemented in FE code and experimentally identified). The mechanical model used are relatively simple since the objective of this study is to explain physical phenomena observed on a large kind of multiscale foam and not necessary to reproduce the real macroscopic response of a specific cellular material. A design of experiment was established to better identify the influence of each parameter - thickness of the wall, density of the central bead and mean strain- on the local response of the multiscale structure. From these results, it seems obvious that these thicker walls constitute a secondary network more rigid and have a strong influence on the macroscopic response of the foam and also on the local deformation of the microstructure (at the cell scale). A first effect of coupling between the two scales has been revealed: For low value of wall thickness, multi mode buckling observed experimentally has been reproduced. This kind of deformation has been generated for the wall of two beads of similar density. The single mode buckling appears for beads of different density. A second effect can be considered in analysing the propagation of the damage in the structure which can correctly explain the occurrence of strain localisation band. The stress field depends on the rigidity of the wall (and then of their thicknesses) and the behaviour of the porous interior of the beads. During compression, this heterogeneous stress field can be strongly perturbed by the two kind of mechanical instabilities of wall buckling or plasticity of the porous interior of the bead. When one of these instabilities appears such as the plastic strain of the porous bead (which can be also considered as buckling at the cell wall scale), it initiates a strong variation of the force field in the vicinity of the damaged zone and exacerbates second instability in bead wall. This propagation of the damage in the multiscale structure of this foam can explain the strain localisation band which is classically observed experimentally.

To conclude on this first step of this study, multiscale physical phenomena observed experimentally in dynamic compression of polymeric foams have been reproduced in using simple models representing the two scales of the foam. Strain localisation has been highlighted in considering the porous interior of beads as a homogeneous material. The second step of the numerical approach will be to introduce the heterogeneity of the microstructure of the cellular beads (in modelling variability in the cell size and defaults such as large bubbles). Discrete Element Modelling (DEM) can be a way to introduce a realistic microscopic cell structure. A modelling using DEM is in progress to reproduce the variability of the cell microstructure, the main difficulty will be the integration of the DEM modelling of the cell microstructure in a FE meshed structure representing the dense wall structure of the beads. The objective of the next step is to model a real structure of polymeric foam and to compare the numerical results with the behaviour of the real sample. Polypropylene foam samples were tested under dynamic compression, the sample structures were measured before and after several step of the dynamic loading in using micro tomographic techniques [14]. The reconstruction of the 3-D images were done and it is now necessary to obtain a good 3-D image of the bead wall structure, requiring the extraction of the bead thick walls from the multiscale structure. This study presented in this paper had shown the strong influence of the wall thickness and the density of the beads. The identification of these parameters is in

progress, the results waited from these reconstruction methods would be used to model more reliably the correlation between the local deformation of the structure and the macroscopic response of the material.

5. REFERENCES

[1]. L. Gibson, M. Ashby, Cellular solids. Structure and properties., 2nd Edition, Cambridge Solid State Science Series, Cambridge University Press, 1997.
[2]. N. Mills, C. Fitzgerald, A. Gilchrist, R. Verdejo, Polymer foams for personal protection: cushions, shoes and helmets, Compos Sci Technol 63 (16) (2003) 2389–2400. doi:doi:10.1016/S0266-3538(03)00272-0.
[3]. T. Triantafillou, J. Zhang, T. Shercli_, L. Gibson, M. Ashby, Failure surfaces for cellular materials under multiaxial loads. ii. comparisons of models with experiment, Int J Mech Sci 31 (9) (1989) 665–678. doi:doi:10.1016/S0020-7403(89)80002-5.
[4]. J. Zhang, N. Kikuchi, V. Li, A. Yee, G. Nuscholtz, Constitutive modeling of polymeric foam material subjected to dynamic crash loading, Int J Imp Eng 21 (5) (1998) 369–386. doi:doi:10.1016/S0734-743X(97)00087-0.
[5]. R. Bouix, P. Viot, J.-L. Lataillade, Polypropylene foam under dynamic loadings: strain rate, density and microstructure effects, Int J Imp Eng 36 (2) (2009) 329–342. doi:doi:10.1016/j.ijimpeng.2007.11.007.
[6]. H. Jin, W.-Y. Lu, S. Sche_el, T. Hinnerichs, M. Nielsen, Full-field characterization of mechanical behavior of polyurethane foams, Int J Solid Struct 44 (21) (2007) 6930–6944. doi:doi:10.1016/j.ijsolstr.2007.03.018.
[7]. C. Chen, V. Deshpande, N. Fleck, A constitutive model for a transversely isotropic compressible solid: user manual for a umat in abaqus., Tech. Rep. CUED/C-MICROMECH/TR.93, Cambridge University, Engineering Department (2003).
[8]. O. Hallquist, Ls-dyna3d theoritical manual., Tech. Rep. Report 1018, LSTC (1994).
[9]. P. Viot, F. Beani, J.-L. Lataillade, Polymeric foam behavior under dynamic compressive loading, J Mater Sci 40(2005) 5829–5837. doi:10.1007/s10853-005-4998-5.
[10]. A. Kraynik, W. Warren, The elastic behavior of low density cellular plastics, Chapmann and Hall, London, 1994, Ch. 7- Low density cellular plastics.
[11]. N. Mills, A. Gilchrist, Properties of bonded-polypropylene-bead foams: data and modelling, J Mater Sci 42 (2007)3177–3189. doi:10.1007/s10853-006-1357-0.
[12]. A. Roberts, E. Garboczi, Elastic properties of model random 3-d open-cell solids, J Mech Phys Solid 50 (2002) 33–55. doi:doi:10.1016/S0022-5096(01)00056-4.
[13]. N. Mills, Bead foam microstructure and processing, Polymer Foams Handbook (2007) 69–83.
[14]. P. Viot, E. Plougonven, D. Bernard, Microtomography on polypropylene foam under dynamic loading: 3d analysis of bead morphology evolution, Compos A: Appl Sci Manuf 39 (8) (2008) 1266–1281. doi:DOI:10.1016/j.compositesa.2007.11.014.
[15]. P. Viot, R. Bouix, I. Iordano_, J.-L. Lataillade, Deformation localisation modelling of polymer foam microstructure under compression: A new approach by discrete element modelling, Compos Struct 92 (2) (2010) 585–592. DOI:10.1016/j.compstruct.2009.09.008.
[16]. B. Croop, H. Lobo, Selecting material models for the simulation of foams in ls-dyna, in: Proceedings of 7th European LS-DYNA Conference, Salzburg, 2009.
[17]. P. Viot, K. Shankar, D. Bernard, E_ects of strain rate and density on dynamic behavior of syntactic foam, Compos Struct 86 (4) (2008) 314–327. doi:doi:10.1016/j.compstruct.2008.07.021.
[18]. G. Liu, Z. Lin, Y. Bao, Improving dimensional accuracy of a u-shaped part through an orthogonal design experiment, Finite Elem Anal Des 39 (2) (2002) 107–118. doi:doi:10.1016/S0168-874X(02)00072-0.